KSME Journal, Vol. 8, No. 3, pp. 219~230, 1994

Numerical Simulation of Fully Developed Flow and Heat Transfer Characteristics in a Curved Tube with Pulsating Pressure Gradient

Young-Ryoul Back,* Jae-Heon Lee, Byung-Ha Kang*** and Myung-Do Oh******

(Received September 18, 1993)

Characteristics of fluid flow and convective heat transfer of a pulsating flow in a curved tube have been investigated numerically. The tube wall is assumed to be maintained at a uniform temperature peripherally in a fully developed pulsating flow region. The temperature and flow distributions over a cross-section of a curved tube with the associated velocity field need to be studied in detail. This problem is of particular interest in the design of Stirling engine heat exchangers and in understanding the blood flow in the aorta. The time-dependent, elliptic governing equations are solved, employing finite volume technique. The periodic steady state results are obtained for various governing dimensionless parameters, such as Womersley number, pulsation amplitude ratio, curvature ratio and Reynolds number. The numerical results indicate that the phase difference between the pressure gradient and averaged axial velocity increases gradually up to $\pi/2$ as Womersley number increases. However, this phase difference is almost independent of the amplitude ratio of pulsation. It is also found that the secondary flow patterns are strongly affected by the curvature ratio and Reynolds number. These, in turn, give a strong influence on the convective heat transfer from the pipe wall to the pulsating flow. The results obtained lead to a better understanding of the underlying physical process and also provide input that may be used to design the relevant system. The numerical approach is discussed in detail, and the aspects that must be included for an accurate simulation are discussed.

Key Words: Pulsating Curved Tube, Numerical Heat Transfer, Secondary Flow

Nomenclature

A : Cross-section area
a : Tube radius
c_p : Specific heat
k : Thermal conductivity
K : Amplitude ratio of pulsation
Nu : Local Nusselt number
$\overline{Nu}_s$: Peripherally averaged Nusselt number
$\overline{Nu}_{t-s}$: Phase and peripherally averaged Nusselt number in a periodic cycle
n : Dimensionless temperature
P : Pressure
Pr : Prandtl number
R_o : Curvature radius
r : Radial Coordinate
Re : Reynolds number
S : Surface area of tube
T : Physical temperature
t : Time
U : Circumferential velocity
V : Radial velocity
W : Axial velocity
$\overline{W}_s$: Cross-section averaged axial velocity

*Graduate School, Hanyang University
** Department of Mechanical Engineering, Hanyang University 17 Haengdang-Dong, Sungdong-Ku, Seoul 133-791, Korea
***Thermal/Fluids Engineering Lab. Korea Insititute of Science and Technology (KIST) P.O. Box 131 Cheongyang, Seoul, Korea
****Mechanical Engineering Research Center, Korea Academy of Industrial Technology, 371-36 Garibong-Dong, Guro-Gu, Seoul 152-120, Korea

Greek characters

α : Thermal diffusivity
β : Womersley number
δ : Curvature
ϕ : Axial coordinate
λ : Phase angle
μ : Viscosity
θ : Circumferential coordinate
ρ : Density
τ : Dimensionless time
ν : Dynamic viscosity
ω : Pulsation frequency

Superscripts

$*$: Dimensional properties
$-$: Average value

Subscripts

s : Peripherally averaged
$t-s$: Time and peripherally averaged
st : Value at non-pulsating steady state

1. Introduction

A large number of practical and fundamental situations involve fluid flow and convection heat transfer associated with a pulsating flow in a curved, heated tube. Such circumstances arise when pulsating pressure gradient is imposed on a flow in a curved, heated tube. The secondary flow occurs in a curved tube by the centrifugal force while this phenomenon is not seen in the straight tube. The secondary flow created by centrifugal force in a curved tube may enhance the convective heat transfer at the tube wall than that in the straight tube even though the pressure drop of the flow is increased. Therefore, to provide the optimum condition in the relevant systems with pulsating flow, the physical phenomena must be investigated for various parameters of the processes. The effect of pulsation frequency, pulsation amplitude, and curvature ratio on flow patterns and heat transfer rate are of particular importance in the design of Stirling engine heat exchangers and in understanding the blood flow in the aorta(1990).

Considerable work has been done on the pulsating flow in a curved tube by several investingators. Dean(1927) carried out a pioneering study analytically on flow characteristics in a curved tube. Hamakiotes and Berger(1990) studied numerically flow profile in the blood vessel, on fully developed region of periodic mass flow through a curved tube. Lyne(1970) predicted the characteristics of pure oscillating flow in the range of low frequency by the theoretical method. He reported the occurrence of an additional pair of secondary flow in the invicid core, which differs from Dean type vorticities. He postulated that this secondary flow is caused by shear action.

Not much attention has been given to the heat transfer characteristics of pulsating flow in a curved tube. Zapryanov and Christov(1979) have obtained a numerical solution on the flow and the thermal field, which are fully developed, in a curved tube. However, these results are obtained by neglecting the time dependency. Simon and Chang(1977) investigated analytically characteristics of heat transfer in a curved tube with pulsating flow. They reported that the time averaged Nusselt number in a curved tube with pulsating is larger than that in a straight pipe with pulsating. Rabadi et al. (1982, 1980) studied numerically characteristics of flow and heat transfer in a curved tube, maintained at peripherally uniform temperature. They found that the time and peripheral average Nusselt number increases as pulsating frequency or Prandtl number increases. However, most of studies were limited to the small curvature of curved tube or low pulsating frequency. The aim of the present study is to investigate heat transfer characteristics in a curved tube with pulsation for various parameters such as high Womersley number and large curvature ratio.

The present study is directed at a numerical simulation on convective heat transfer characteristics of a pulsating flow in a curved tube. The tube is assumed to be maintained at a uniform tempe rature peripherally in a fully developed pulsation flow region. The time-dependent, two-dimensional, elliptic governing equations are solved, employing finite volume technique. The effect of various dimensionless parameters such as pulsating frequency, amplitude of pulsation, cur-

vature ratio and Reynolds number on the flow and thermal field and the corresponding heat transfer rate from the heated wall to the pulsating flow are investigated in detail. The results obtained lead to a better understanding of the underlying physical process and are important in the design of the relevant systems.

2. Physical Model and Analysis

The physical model and coordinate system considered are shown in Fig. 1. The tube radius and curvature radius of a curved tube are "a" and "R_0," respectively. The flow in a curved tube is assumed to be periodically developed by the periodic axial pressure gradient with time. Accordingly, the velocity distributions at any cross section are same regardless of the axial direction position but vary with time. Tabolt and Gong(1983) have confirmed experimentally that a periodic flow entering a curved tube become fully developed, in the sense that it becomes periodic in time at any cross-section, and indenpendent of axial position at some downstream position depending on curvature ratio, frequency parameter and Reynolds number. Hamakiotes & Berger (1990) compared the numerical results to be computed from the assumption of laminar flow with Tabolt & Gong's(1983) experimental data. He confirmed that the flow patterns for Re=500 are in very good qualitative and quantitative agreement with experimental data. From this physical consideration, we assumed that flow in a curved tube is laminar. The present problem, therefore is a two-dimensional one treating only this fully developed region. Despite of two dimensionality of the problem, there are three velocity components to deal with and all momentum equations are required.

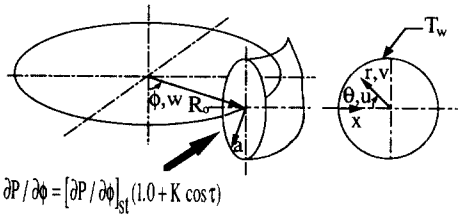

Fig. 1 Physical model and toroidal coordinate system for a curved pipe

The thermal boundary conditions chosen in the present study assume that the wall temperature, T_w varies linearly along the axial direction but is uniform peripherally and constant with time. For above thermal boundary condition, the axial directional gradient of the fluid temperature, $\partial T/\partial\phi$ is constant at regime except the entrance region. That is, temperature field is fully developed and the distribution of the dimensionless temperature, "n" defined as Eq. (1) is same regardless of the axial position except the entrance region.

$$n=\frac{T_w-T}{a(\partial T/\partial\phi)}R_0 \tag{1}$$

The coordinate system used in the present study is toroidal coordinate, in which a point inside the tube could be specified by the three orthogonal coordinates, θ, r and ϕ, and the corresponding velocity components would be U, V and W, respectively. The following assumptions are introduced in the present study.

1. All the properties of fluid are constant.
2. The flow and temperature field are fully developed
3. The flow is incompressible and laminar.
4. The pitch effect of a curved tube is ignored.

The governing equations simplified by the above assumptions are expressed as follows;

Continuity equation

$$\frac{1}{r}\frac{\partial}{\partial r}(rV)+\frac{1}{r}\frac{\partial U}{\partial\theta}+EF=0 \tag{2}$$

Momentum equations

$$\begin{aligned}&\beta^2\frac{\partial U}{\partial\tau}+V\frac{\partial U}{\partial r}+\frac{U}{r}\frac{\partial U}{\partial\theta}+\frac{UV}{r}-EW^2\sin\theta\\&=-\frac{1}{r}\frac{\partial P}{\partial\theta}+\Big\{\frac{1}{r}\frac{\partial}{\partial r}(r\frac{\partial U}{\partial r})+\frac{1}{r^2}\frac{\partial^2U}{\partial\theta^2}-\frac{U}{r^2}\\&\quad+\frac{2}{r^2}\frac{\partial V}{\partial\theta}-E\cos\theta\frac{\partial U}{\partial r}+E\sin\theta\\&\quad(\frac{1}{r}\frac{\partial U}{\partial\theta}+\frac{V}{r})-E^2F\sin\theta\Big\}\end{aligned} \tag{3}$$

$$\begin{aligned}&\beta^2\frac{\partial V}{\partial\tau}+V\frac{\partial V}{\partial r}+\frac{V}{r}\frac{\partial V}{\partial\theta}-\frac{U^2}{r}+EW^2\cos\theta\\&=-\frac{\partial P}{\partial r}+\Big\{\frac{1}{r}\frac{\partial}{\partial r}(r\frac{\partial V}{\partial r})+\frac{1}{r^2}\frac{\partial^2V}{\partial\theta^2}-\frac{V}{r^2}\end{aligned}$$

$$-\frac{2}{r^2}\frac{\partial U}{\partial\theta}+E\left(-\cos\theta\frac{\partial V}{\partial r}+\frac{\sin\theta}{r}\frac{\partial V}{\partial\theta}-\frac{U\sin\theta}{r}\right)+E^2F\cos\theta\Big\} \quad (4)$$

$$\beta^2\frac{\partial W}{\partial\tau}+V\frac{\partial W}{\partial r}+\frac{U}{r}\frac{\partial W}{\partial\theta}+EFW = -E\frac{\partial P}{\partial\phi}+\left\{\frac{1}{r}\frac{\partial}{\partial r}\left(r\frac{\partial W}{\partial r}\right)+\frac{1}{r^2}\frac{\partial^2 W}{\partial\theta^2}-E^2W+E\left(-\cos\theta\frac{\partial W}{\partial r}+\frac{\sin\theta}{r}\frac{\partial W}{\partial\theta}\right)\right\} \quad (5)$$

Energy equation

$$\beta^2\frac{\partial n}{\partial\tau}+V\frac{\partial n}{\partial r}+\frac{U}{r}\frac{\partial n}{\partial\theta} = EW+\frac{1}{Pr}\left\{\frac{1}{r}\frac{\partial}{\partial r}\left(r\frac{\partial n}{\partial r}\right)+\frac{1}{r^2}\frac{\partial^2 n}{\partial\theta^2}+E\left(\frac{\sin\theta}{r}\frac{\partial n}{\partial\theta}-\cos\theta\frac{\partial n}{\partial r}\right)\right\} \quad (6)$$

where, E and F are;

$E=\delta/(1-\delta r\cos\theta)$, $F=U\sin\theta-V\cos\theta$

In Eq. (5), the axial pressure gradient, which is the driving force of main flow, is expressed as follows;

$$\partial P/\partial\phi=[\partial P/\partial\phi]_{st}[1.0+K\cos(\tau)] \quad (7)$$

This means that the driving force is a sinusoidally varying axial pressure gradient with time imposed on a steady component$(\partial P/\partial\phi)_{st}$. In above Eq. (7), "K" is the ratio of the maximum amplitude of time varying component to the steady component. A very small value of pulsation amplitude, K means quasi-steday state. The dimensionless variables are defined as below.

$$r=\frac{r^*}{a},\ \tau=\omega t,\ U=\frac{U^*}{(\nu/a)},\ V=\frac{V^*}{(\nu/a)},\ W=\frac{W^*}{(\nu/a)},\ P=\frac{P^*a^2}{\rho\nu^2},\ \alpha=\frac{k}{\rho c_p},\ Pr=\frac{v}{\alpha},\ v=\frac{\mu}{\rho},\ \delta=\frac{a}{R_0},\ \beta=a(\omega/v),^{1/2}\ Re=\frac{aW_{st}{}^*}{\nu}. \quad (8)$$

In above equations, the starred marks indicate the dimensional variables, ω is the angular velo city of pulsation, μ is viscosity, ν is the dynamic viscosity, Pr is Prandtl number, α is the thermal diffusivity and Re is Reynolds number. Reynolds number is computed by referring the cross section average velocity $W_{st}{}^*$ resulting from the steady pressure gradient, $(\partial P/\partial\phi)_{st}$ given as the input condition. Therefore, if the steady component of the axial pressure gradient, $(\partial P/\partial\phi)_{st}$ is given as input condition for the steady state, the Reynolds number is obtained from the numerical calculation for the given curvature ratio. Later, the discussions will be performed for Reynolds number instead of the axial pressure gradient, $(\partial P/\partial\phi)_{st}$ used as input condition.

Square of Womersley number, β^2 is the ratio of the characteristic time, a^2/v to the characteristic oscillating time, $1/\omega$. This parameter also be interpretted as the ratio of the tube radius "a" to the Stokes layer thickness (v/ω).[1/2] Accordingly, we use a^2/v as the characteristic time scale for solving numerically the present problem. In case of Womersley number, $\beta=0$, the pulsation frequency is equal to "0," it means that the pulsation period is infinite. Womersley number, β and pulsation amplitude, K play an important role in heat and mass transfer in pulsating flow field. The pulsation amplitude, K is the ratio of the alternating to the steady component of the axial pressure gradient.

The boundary conditions in terms of dimensionless quantities were obtained from the physical boundary conditions. The resulting dimensionless boundary conditions are expressed as follow;

$$U=\frac{\partial V}{\partial\theta}=\frac{\partial W}{\partial\theta}=\frac{\partial n}{\partial\theta}=0 \quad \text{at the } \theta=0 \text{ and } \theta=\pi$$

$$U=V=W=n=0 \quad \text{at the wall}$$

$$\frac{\partial U}{\partial r}=\frac{\partial V}{\partial r}=\frac{\partial W}{\partial r}=\frac{\partial n}{\partial r}=0 \quad \text{at } r=0 \quad (9)$$

The accurate initial conditions are required in the analysis of unsteady problems. Since the pulsating flow considered in this study is steady periodic flow, the solution of nonpulsating, steady state is used as the initial condition in the present numerical approach to reduce the computation time to reach the steady periodic state.

3. Numerical Scheme

In all cases considered here, the numerical calculations were carried out for a half of tube cross-section, because the flow and temperature field are fully developed and the geometry of present model is symmetric. The discretization is based on the finite volume method of Patankar(1980). The non-uniform staggered 15x15 grid system was used to discretize the governing equations. Because the flow is unsteady during a cycle, each cycle was subdivided into 200 time steps. In each time step, the converged solution is obtained when the relative error of dependent variables are less than 10^{-4} and local mass flux residual is reached to 10^{-5} during an iterative calculation. The effects of the chosen numerical parameters, such as grid size, time step and convergence criterion are also studied to ensure a negligible effect on the computed steady periodic state results. The effect of grid dependency were studied. Increasing the mesh point to 15x19 changes the result only very slightly(less than 2% for axial velocity). The number of iteration depends on Womersley number, pulsating amplitude, Reynolds number and curvature ratio. The underrelaxation method was employed in present calculation to achieve the numerical stability of solution. The underrelaxation factors for U, V, W, P and T are 0.5, 0.5, 0.8, 0.8 and 0.8, respectively.

A major difficulty in the numerical solution of the present problem lies in facts that the initial condition are not known a priori, which neccessitates an interative solution on the entire cycle. The estabilishment of inaccurate initial condition needs 10~20 cycles to gain the steady periodic state solution in the range of present calculation. It was found that the iterative number of cylcle required for the periodic solution is increased as Womersley number is increased, while it is independent of curvature ratio, amplitude ratio and Reynolds number.

4. Numerical Results and Discussion

Fluid flow and convective heat transfer of the pulsation flow on a curved tube have been investigated by numerical simulation for various parameters. The reference governing parameters were selected as $\beta=0.8$, $K=1.5$, $\delta=0.01$ and $Re=500$ for the convenience of discussion. The working fluid used in the present calculation was air ($Pr=0.7$). On the basis of above reference condition, the numerical calculations were carried out for 18 cases. A complete list of all the parameters for 18 cases calculated in present study is given in Table 1. All the results obtained in numerical calculation will be discussed, comparing with reference condition.

Table 1 Run numbers of present study

Re	δ	K	β	$(\partial P/\partial\phi)_{st}$
500	0.01	1.5	2	-5.92×10^{3}
500	0.01	1.5	4	-5.92×10^{3}
500	0.01	1.5	6	-5.92×10^{3}
*500	0.01	1.5	8	-5.92×10^{3}
500	0.01	1.5	10	-5.92×10^{3}
500	0.01	1.5	12	-5.92×10^{3}
500	0.01	1.5	14	-5.92×10^{3}
500	0.01	0.5	8	-5.92×10^{3}
500	0.01	2.5	8	-5.92×10^{3}
500	0.01	3.5	8	-5.92×10^{3}
500	0.01	4.5	8	-5.92×10^{3}
500	0.05	1.5	8	-7.63×10^{3}
500	0.075	1.5	8	-8.17×10^{3}
500	0.1	1.5	8	-8.58×10^{3}
100	0.01	1.5	8	-8.19×10^{2}
300	0.01	1.5	8	-3.10×10^{3}
800	0.01	1.5	8	-1.09×10^{4}
1000	0.01	1.5	8	-1.48×10^{4}

* Reference condition

4.1 Flow characteristics

Cross-section average of axial velocity is defined, in order to observe the time variationof axial velocity during a cycle, as follows;

$$\bar{W}_s = \int_A W\, dA \,/ \int_A dA \tag{10}$$

Figure 2 shows the computed cross-section average axial velocity defined in Eq. (9) during a cycle and the axial driving pressure gradient with time(phase angle), for $\beta=2.0$, 8.0 and 14.0, at $K=1.5$, $Re=500$ and $\delta=0.01$. In this figure, it is observed that the time variation of axial velocity during a cycle is significant with small Womersley number($\beta=2.0$), while it becomes meager with the increased Womersley number. And it is also seen from this figure that the phase difference between pressure gradient and axial velocity becomes larger as the Womersley number is increased. This phase difference is about $\pi/2$ for the case of $\beta=14$. This result indicates that the pressure gradient leads $\pi/2$ than the axial velocity for the high Womersley number. This result is caused by the increase of time variation rate of pressure gradient with the increased Womersley number. The similar qualitative tendency is also observed from the results of Berger(1990), who studied pulsating flow with the sinusoidal mass-flow rate in a curved tube. In case of $\beta=2.0$, it can be seen that the axial velocity changes from the natural flow into the reverse flow at phase angle, $\lambda=\pi$. This phenomenon is because the axial driving pressure gradient changes from the favorite pressure gradient into the unfavorite pressure gradient at $\lambda=\pi$. For high frequency such as $\beta=8.0$ or 14.0, the reverse flow could not be observed due to the reduction of amplitude ratio of axial velocity. The reverse flow appeared at $\lambda=\pi$ in case of $\beta=2.0$, continues until phase angle, $\lambda=3\pi/2$ and axial flow is changed from the reverse flow into natural flow at $\lambda=3\pi/2$.

Figures 3 and 4 show the distribution of instantaneous axial velocity along the symmetric line during a cycle at $K=1.5$, $\delta=0.01$ and $\mathrm{Re}=500$ for $\beta=2.0$ and $\beta=8.0$, respectively. We can predict that time gradient of physical properties during a cycle are steepest at the typical phase angles, such as $\lambda=0$, $\lambda=\pi/2$, $\lambda=\pi$ and $\lambda=3\pi/2$. Accordingly, all the results will be discussed for these phase angles. As shown in Fig. 3, the axial velocity has the largest value in the vicinity of the outer wall at phase angle $\lambda=0$ by driving the largest axial pressure gradient. The steep gradient of axial velocity in this region is desirable for increasing the convective heat transfer as will be seen later. The distribution of axial velocity at $\lambda=\pi/2$ is similar to that at $\lambda=0$ however, the quantitative values of axial velocity are smaller than those at $\lambda=0$. The axial velocity distribu-

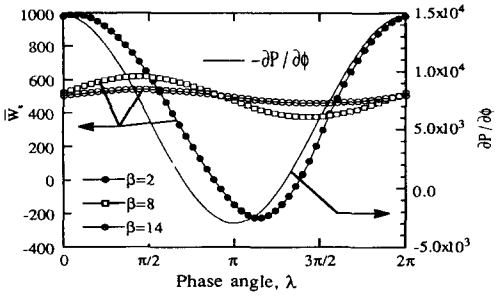

Fig. 2 Dimensionless cross section averaged axial velocity and pressure gradient during a cycle

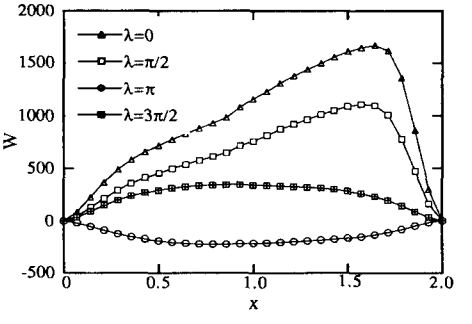

Fig. 3 Dimensionless axial velocity along the horizontal diameter at $\mathrm{Re}=500$, $K=1.5$, $\beta=2.0$ and $\delta=0.01$

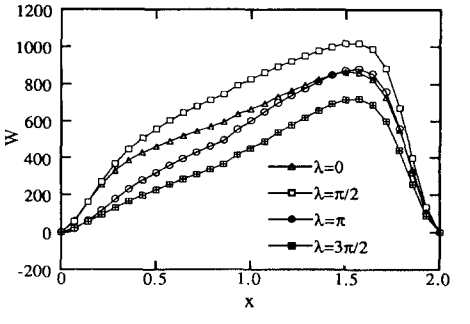

Fig. 4 Dimensionless axial velocity along the horizontal diameter at $Re=500$, $K=1.5$ and $\beta=8.0$, $\delta=0.01$

tions at $\lambda=\pi$ and $\lambda=3\pi/2$ are very different from those at $\lambda=0$ and $\lambda=\pi/2$. This is due to a decrease of axial driving pressure gradient at $\lambda=\pi$ and $\lambda=3\pi/2$. In particular, the reverse flow appears at $\lambda=\pi$ by means of driving the largest unfavorite pressure gradient. From this result, we can predict that the axial reverse flow appears in all the region at $\lambda=\pi$ for low Womersley number.

In Fig. 4, the axial velocity distribution is qualitativley similar to that of $\lambda=0$ and $\lambda=\pi/2$ in Fig. 3. However, the reverse flow is not observed in Fig. 4 in this case. This is due to a decrease of axial velocity amplitude ratio with the increased Womersley number. From this result, we can see that the amplitude ratio and axial velocity during a cycle decreases as Womersley number increases.

To visualize the secondary flow originated by centrifugal force, the distributions of streamlines and velocity vectors for $\beta=2.0$ and $\beta=8.0$ are shown in Figs. 5 and 6 respectively. In Fig. 5, as the phase angle varies, the flow field is differently distributed and the strength of secondary flow is the most intense at $\lambda=0$ and the smallest at $\lambda=\pi$. This is, as illustrated in Figs. 3 and 4 due to the time variation of axial velocity. In Fig. 6, it is found that the time variation of secondary flow during a cycle is smaller than that in Fig. 5. From above results, we can predict that time variation of temperature is meager for high Womersley number and is intense for low Womersley number.

The time variation of cross-section averaged axial velocity at $\delta=0.01$, $Re=500$ and $\beta=8.0$ is shown for various pulsation amplitude ratio K in Fig. 7. It is observed that the axial velocity during a cycle is periodic and the phase difference between the driving axial pressure gradient and axial velocity is about $\pi/2$, regardless of amplitude ratio K. This phenomenon is because the Womersley number is given at 8.0 for the cases considered. From this result, it is induced that the phase difference between axial velocity and axial driving pressure gradient is negligibly affected by the amplitude ratio K.

Figure 8 shows the distribution of instantaneous axial velocity along the symmetric line at a given amplitude ratio $K=3.5$ for the several

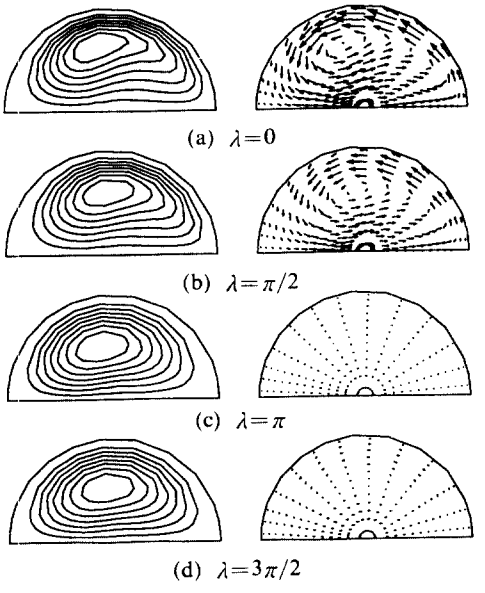

Fig. 5 The distributions of streamlines and velocity vectors at $Re=50$, $K=1.5$, $\beta=2.0$ and $\delta=0.01$

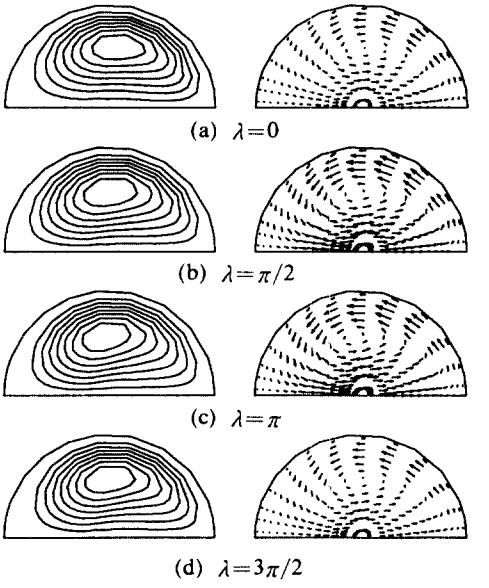

Fig. 6 The distributions of streamlines and velocity vectors at $Re=500$, $K=1.5$, $\beta=8.0$ and $\delta=0.01$

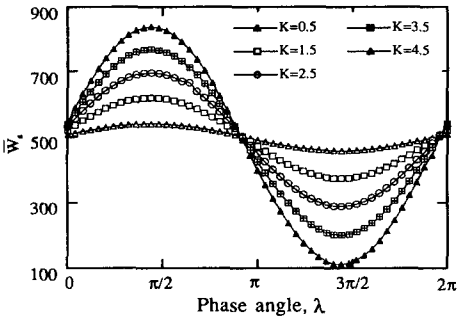

Fig. 7 Dimensionless cross section averaged axial velocity for various amplitude ratio during a cycle at $Re=500$, $\beta=8.0$ and $\delta=0.01$

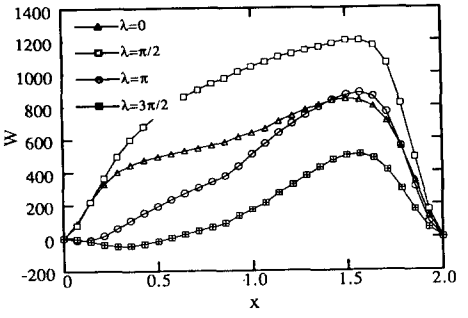

Fig. 8 Dimensionless axial velocity along the horizontal diameter at $Re=500$, $K=3.5$, $\beta=8.0$ and $\delta=0.01$

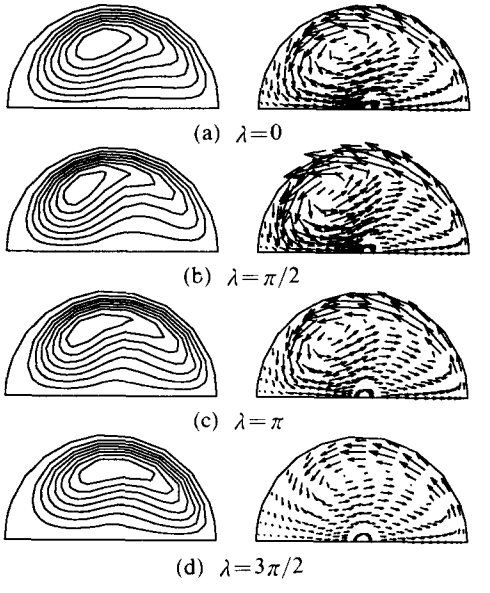

Fig. 9 The distributions of streamlines and velocity vectors $Re=500$, $K=1.5$, $\beta=8.0$ and $\delta=0.075$

phase angles. As shown in Fig. 8, the time variation of axial velocity is more substantial than that of reference condition seen in Fig. 4. In particular, the weak reverse flow appears in the region near the inner wall and the natural flow appears in the region of invicid core and in the region near the outer wall at phase angle $\lambda=3\pi/2$ with minimum axial velocity. It can be predicted that the convective heat transfer could be reduced at the phase angle with a reverse flow. It is observed from the present result that the strength of this reverse flow becomes larger as the amplitude ratio K is increased. The secondary flow is created by the combination of axial velocity and curvature of the curved tube.

When the curvature ratio[δ] is 0.075 and other parameters are equal to reference condition, the distributions of streamlines and velocity vectors at four phase angles are shown in Fig. 9. In this figure, the secondary flow varies strongly with time and the strength of secondary flow is larger than that of reference condition for all phase angles. The strong secondary flow may lead to enhance the convective heat transfer, to be discussed later in detail. And the center of secondary flow moves to inner wall by the increase of centrifugal force.

4.2 Temperature field

Figures 10 and 11 show the typical temperature distributions obtained in the present study. In Fig. 10, it is found that temeperature gradient near the outer wall at $\lambda=0$ and $\lambda=\pi/2$ is steep by strong centrifugal force. Therefore, the temperature field at this phase angle is dominated by convection. While the temperature gradient at $\lambda=\pi$ is meager in the all region, particularly the negative temperature values are observed near the inner wall. The axial reverse flow occurs near to $\lambda=\pi$ in case of the low Womersley number($\beta=2.0$) as illustrated in Fig. 2. This reverse flow by the unfavorite axial pressure gradient is responsible for the existence of fluid heated higher than the wall temperature. In the reverse flow region, this phenomenon appears similarly at $\lambda=3\pi/2$.

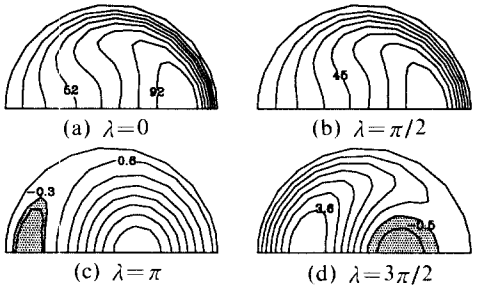

Fig. 10 The distributions of isotherms at $Re=500$, $K=1.5$, $\beta=2.0$ and $\delta=0.01$

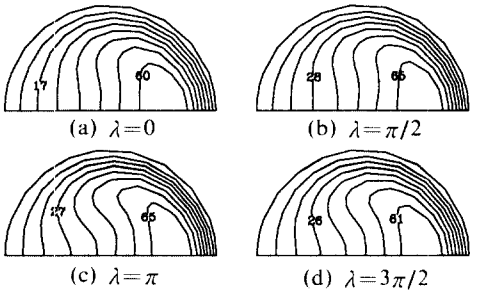

Fig. 11 The distributions of isotherm at $Re=500$, $K=1.5$, $\beta=8.0$ and $\delta=0.01$

In Fig. 11, the isotherms are densly distributed at all the phase angle in the vicinity of the outer wall, and coarsely near the inner wall. This is due to a centrifugal force drived from inner wall into outer wall. Accordingly, one can see that temperature field at all the phase angles during a cycle are strongly dominated by high Womersley number due to convection effect.

4.3 Characteristics of convective heat transfer

Toi investigate characteristics of convective heat transfer in pulsating flow, the local Nusselt number, Nu, peripheral averaged Nusselt number $\overline{Nu}_s$ at any phase, and the phase and peripheral averaged Nusselt number $\overline{Nu}_{t-s}$ are defined as follow.

$$Nu=\frac{2}{n_b}\left[\frac{\partial n}{\partial r}\right]_{r=1} \tag{11}$$

$$\overline{Nu}_s=\frac{1}{\pi}\int_s Nu\ dS \tag{12}$$

$$\overline{Nu}_{t-s}=\frac{1}{2\pi}\int_0^{2\pi}\overline{Nu}_s\ d\lambda \tag{13}$$

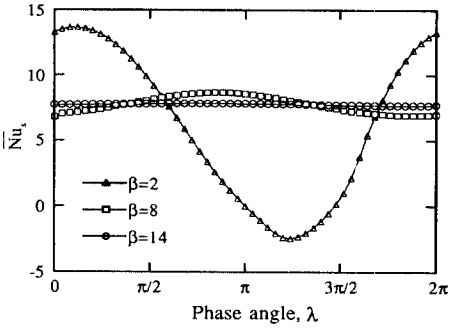

Fig. 12 The peripherally averaged Nusselt number during a cycle at $Re=500$, $K=1.5$ and $\delta=0.01$

Figure 12 illustrates the peripheral averaged Nusselt number $\overline{Nu}_s$ along the phase angle for $\beta=2.0$, $\beta=8.0$ and $\beta=14.0$. As shown in this figure, $\overline{Nu}_s$ varies significantly during a cycle in case of $\beta=2.0$. In this case, the variation trend of $\overline{Nu}_s$ along the phase is similar to that of axial velocity shown in Fig. 2. The negative value of $\overline{Nu}_s$ is observed in the range of $\lambda=\pi$ and $\lambda=3\pi/2$, which is due to the reverse flow. When the Womersley number is 8 or 12, the time variation of Nu during a cycle is relatively flat along the phase angle. This is because the flow distribution along the phase angle is not varied strongly during a cycle.

Figures 13 and 14 show the distributions of local Nusselt number Nu along the periphery for four phase angles at $\beta=2.0$ and $\beta=8.0$, respectively. In these figures, "0" and "π" denote the inner and outer wall, respectively. In Fig. 13, the time variation of Nu in the vicinity of the outer wall is very large because the thermal field near the outer wall varies substantially with time. The value of Nu at $\lambda=0$ and $\lambda=\pi/2$ is much larger in the outer wall, compared with that in the inner wall, due to the counter clockwise secondary flow. The distribution of Nu at $\lambda=\pi$ and $\lambda=3\pi/2$ is flat and the value is nearly "0". This is due to the reduction of convective effect at $\lambda=\pi$ and $\lambda=3\pi/2$. As shown in Fig. 14 for high Womersley number, it is clear that the time variation of Nu is small because the secondary flow varies little during a cycle. The heat transfer

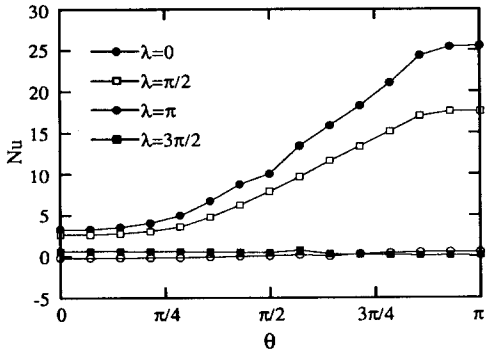

Fig. 13 The distributions of local Nusselt number along pipe surface at $Re=500$, $K=1.5$, $\beta=2.0$ and $\delta=0.01$

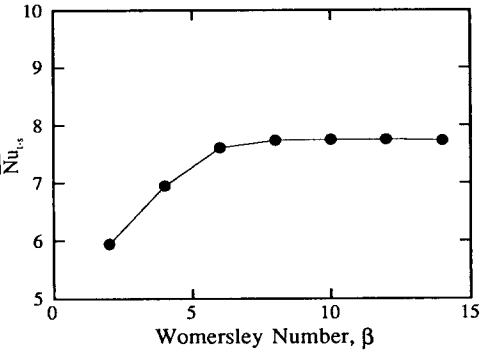

Fig. 15 Time and peripherally averaged Nusselt number as a function of Womersley number at $Re=500$, $K=1.5$ and $\delta=0.01$

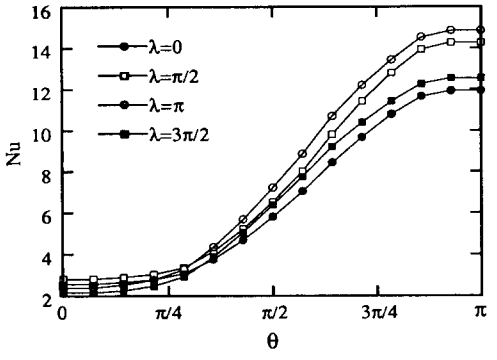

Fig. 14 The distributions of local Nusselt number along pipe surface at $Re=500$, $K=1.5$, $\beta=2.0$ and $\delta=0.01$

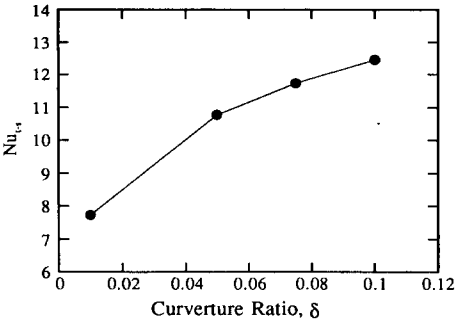

Fig. 16 Time and peripherally averaged Nusselt number as a function of curvature ratio at $Re=500$, $K=1.5$ and $\beta=8.0$

characteristics of these cases are strongly affected by the convection.

The Womersley number(β), pulsation amplitude(K), curvature ratio(δ) and Reynolds number(Re) play important roles in pulsating flow in a curved tube. Figures 15 and 16 show the behavior of the time and peripheral averaged Nusselt number $\overline{Nu}_{t-s}$ for various dimensionless parameters. It is obvious from Fig 15. When Womersley number is small, the time and peripheral averaged Nusselt number $\overline{Nu}_{t-s}$ is smaller than that of high Womersley number, and increases asymtotically up to 7.69 with increasing Womersley number. This is because, for low Womersley number the time variation of flow during a cycle is stronger than that for high Womersley number, in particular, the axial reverse flow appears in case of $\beta=2.0$, as illustrated in Fig. 2

The effect of curvature ratio on $\overline{Nu}_{t-s}$ is shown in Fig. 16 In this figure, the phase and peripheral averaged Nusselt number is almost increased linearly by means of augmentation of centrifugal force. It is easily predicted that the strength of secondary flow becomes much stronger with the increase of curvature, and consequently the convective heat transfer rate in a curved tube is increased. When the curvature ratio is increased from 0.01 to 0.1 as 10 times, the increment rate of $\overline{Nu}_{t-s}$ is approximately 60%. It was confirmed that the variation of time and peripheral averaged Nusselt number as a function of Reynolds number is nearly similar to that of curvature ratio. That is, the time and peripheral averaged Nusselt number increases with the

increase of Reynolds number. The distribution of $\overline{Nu}_{t-s}$ as a function of Reynolds number is shown in Fig. 17, when curvature ratio(δ), amplitude ratio(K) and Womersley number(β) are 0.01, 1.5 and 8.0, respectively. As shown in this figure, $\overline{Nu}_{t-s}$ is increased almost linearly by an increase of centrifugal force as Reynolds number is increased. One can see from these gualitative results that $\overline{Nu}_{t-s}$ is strongly influenced by means of centrifugal force, which is originated curvature and axial flow(Reynolds number).

Figure 18 illustrates the variation of time and peripheral averaged Nusselt number with amplitude ratio. It is seen from this figure that $\overline{Nu}_{t-s}$ are not change much, regardless of a variation of amplitude ratio. This is because flow characteristics are not affected by amplitude ratio, when Womersley number is large(8.0). It is predicted,

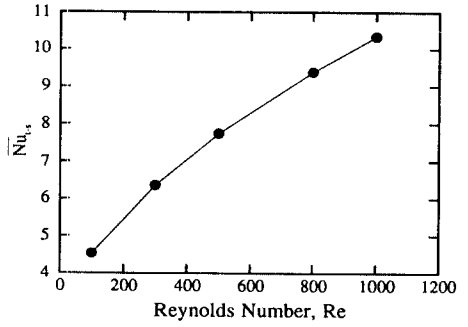

Fig. 17 Time and peripherally averaged Nusselt number as a function of Reynolds number at $K=1.5$, $\beta=8.0$ and $\delta=0.01$

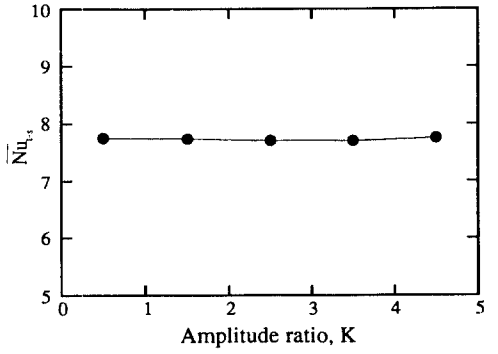

Fig. 18 Time and peripherally averaged Nusselt number as a function of amplitude ratio at $Re=500$, $\beta=8.0$ and $\delta=0.01$

however, that a variation of time and peripheral averaged Nusselt number becomes large in case of small Womersley number.

5. Conclusions

Characteristrics of the pulsating flow and convective heat transfer have been investigated numerically in a curved tube maintained at uniform temperature peripherally for various parameters such as Womersley number, pulsation amplitude, curvature ratio and Reynolds number. The results are summerized as follows.

1. When Womersley number is greater than 8.0, the phase difference between the axial driving pressure gradient and the axial velocity is almost $\pi/2$ and is nearly independent of pulsation amplitude.

2. In case of the low Womersley number, the reverse flow appears in the range of $\lambda=\pi$ and $\lambda=3\pi/2$, and temporal variation of axial and secondary flow is stronger than for high Womersley number.

3. As Womersley number increases, the temporal and peripheral averaged Nusselt number increases asymtotically up to 7.69.

4. The temporal variation of peripheral averaged Nusselt number becomes meager with the increase of Womersley number.

5. It is found that the strength of secondary flow and the temporal and peripheral averaged Nusselt number is augmented with the increased curvature and the increased Reynolds number.

Acknowledgement

Appreciation is expressed to Turbo and Power Machinary Research Center of KOSEF whose support provided the means to accomplish this work.

References

Dean, W. R., 1927, "Note on the Motion of Fluid in a Curved Pipe," Phil, Mag., pp. 208~223.

Hamakiotes, C. and Berger, S. A., 1990, "Periodic Flows Through Cuved Tubes: Th Effect of the Frequency Parameter," J. Fluid Mech. Vol. 210, pp. 353~370.

Lyne, W. H., 1970, "Unsteady Viscous Flow in a Curved Pipe," J. Fluid Mech., Vol. 45, Part 1, pp. 13~31.

Patankar, S. V., 1980, Numerical Heat Transfer and Fluid Flow, McGraw-Hill, New York, pp. 41~60.

Rabadi, N. J., Chow, J. C. F. and Simon, H. A, 1982, "Heat Transfer in Curved Tubes with Pulsating Flow," Int. J. Heat & Mass Transfer. Vol. 25, pp. 195~203.

Rabadi, N. J., Chow, J. C. F. and Simon, H. A., 1980, "Numerical Solution for Fully Developed Laminar Pulsating Flow in Curved Tubes," Num. Heat Transfer., Vol. 3, pp. 225~239.

Simon, H. A., Chang, M. H. and Chow, J. C. F., 1977, "Heat Transfer in Curved Tube Pulsatile, Fully Developed, Laminar Flow," ASME J. of Heat Transfer, Vol. 99, pp. 590~595.

Tabolt, L. and Gong, K. O., 1983, "Pulsatile Entry Flow in a Curved Pipe," J. Fluid Mech., Vol. 128, pp. 1~25.

Zapryanov, Z., Christov, C. and Toshev, E., 1979, "Fully Developed Laminar Flow and Heat Transfer in Curved Tubes," Int. J. Heat & Mass Transfer, Vol. 23, pp. 873~880.